C.P. No. 576

C.P. No. 576

MINISTRY OF AVIATION

AERONAUTICAL RESEARCH COUNCIL

CURRENT PAPERS

Low-Speed Wind-Tunnel Tests on Sharp-Edged Gothic Wings of Aspect-Ratio 3/4

by

R. F. A. Keating

C.P. No.576

U.D.C. No. 533.693.3 : 533.6.013.413

May, 1960

LOW-SPEED WIND-TUNNEL TESTS ON SHARP-EDGED GOTHIC WINGS OF ASPECT-RATIO 3/4

by

R. F. A. Keating

SUMMARY

The results of wind-tunnel tests on a cambered and an uncambered gothic wing are presented. Longitudinal and lateral force measurements were made on both wings, together with oil flow visualisation studies on the cambered wing.

The flow patterns showed that the design requirement of fully attached flow at a small range of incidence of the cambered wing was realised. However, the cambered wing gave less lift than the uncambered version at any prescribed incidence; this loss amounted to $\Delta C_L = -0.13$ at $\alpha = 15^\circ$ i.e. a loss of 27%. A reduction of stability occurs near the design point which is recovered at higher incidences, otherwise the location of the aerodynamic centres of both wings are the same, namely 0.52 c_o from the apex. The higher L/D obtained with the cambered model is associated with the displacement of the incidence for minimum drag towards the design incidence, without much increase in the value of the minimum drag, together with a reduction in lift-dependent drag.

There is only a small difference in the rolling moment derivative between the cambered and the uncambered model when plotted against C_L. However, at the same incidence, the difference is large, $-dC_\ell/d\beta$ being 42% smaller for the cambered wing at 15° incidence.

Previously issued as R.A.E. Tech. Note No. Aero 2686 - A.R.C.22,370.

LIST OF CONTENTS

LIST OF ILLUSTRATIONS

LIST OF ILLUSTRATIONS (Contd)

1 INTRODUCTION

Previous low-speed tunnel tests[1,4] have investigated the characteristics of sharp-edged gothic and delta wings without camber. To provide some indication of the effects of camber, the characteristics of an uncambered sharp-edge gothic wing of aspect ratio 3/4 and 8¼% thick were compared with those of a cambered version, designed by Weber's method[2] to give attached flow at the sharp leading-edge at $C_L = 0.1$.

Longitudinal and lateral force measurements were made on both wings, as well as oil flow experiments on the cambered model to investigate the development of the separations.

The tests were carried out in the 13' × 9' low-speed wind-tunnel at the Royal Aircraft Establishment, Bedford.

2 EXPERIMENTAL DETAILS

The geometry of the models is shown in Fig.1 and the leading dimensions appear in Table 1. The uncambered model was constructed as a sandwich of teak with a Tufnol core which projected to form the sharp edges of the planform. The cambered wing was made of a fibre-glass skin covering a foamed plastic filling*. The models were suspended from the overhead balance by a wire rig and were tested at a speed of 100 ft/sec and a Reynolds number of 3.8×10^6 based on centre line chord. The forces and moments were reduced to coefficients resolved about "stability axes" through the mean quarter chord point. The oil flow experiments were made using the fluorescent technique for visualisation, with anthracene pigment and kerosene.

3 RESULTS AND DISCUSSION

3.1 Flow visualisation

The flow characteristics of the uncambered wings of this type have been fully discussed in Ref.1 and elsewhere, but important differences are to be expected on the cambered wing due to its large side surfaces.

The flow patterns through a range of incidence on the upper surface of the cambered wing are shown in Figs.2 to 4 and on the lower surface in Fig.5. The effect of yaw on the upper surface patterns are shown in Figs.6 to 8.

At $\alpha = 2^\circ$ there is an attachment line on the upper surface and a pair of small vortex patterns[3] on the lower surface. At 4° and 6° the flow appears to be attached at the leading edge but separates above $\alpha = 8^\circ$ with the vortices formed on the upper surface and an attachment line on the lower. The vortex pattern occurs near the leading edge, widening and extending further inboard with increase of incidence. Whenever the flow separates from the leading edge it does so completely, forming a vortex but no mixed flow.

Figs.6 to 8 show the effect of 10° of sideslip at incidence. The first vortex pattern is visible at 4° incidence on the leeward (port) of the leading-edges, with an attachment on the windward (starboard). This vortex grows in size with increasing incidence; its pattern is well defined and slightly narrower than that due to incidence at zero sideslip. The secondary attachment line does not extend as far as the trailing edge and leaves the model on the drooped part of the camber. A vortex does not form on the windward facing

---

* This was an interim model which was produced quickly, but the concessions made in the accuracy of its shape are not considered to have an important effect on the results.

leading edge until 12° incidence and then a separation line can only just be distinguished. A weak vortex from the sharp centre ridge is present at all incidences. The schematic positions of the vortices inferred from surface flow patterns are summarised in Fig.9 showing the flow in a cross-section plane. The cambered model shows large changes in size of the vortices and the vortex patterns of the two models differ greatly when yawed. The flow in the cross-section plane of the cambered model is superficially similar to the flow over a two dimensional inverted U-channel, as the flow on the uncambered model is likewise similar to that of a two dimensional flat-plate wing.

3.2 Lift characteristics

The lift coefficient of the wings are plotted against incidence in Fig.10. The lift-coefficient of the cambered model is considerably lower than the uncambered model at all angles of incidence; at $\alpha = 15^{\circ}$ incidence, for instance, the reduction amounts to $\Delta C_L = -0.13$ or a 27% loss. Inspection of the lift curves shows that they are similar in shape and size but are displaced from each other by the magnitude of the design C_L and incidence. This is shown clearly in Fig.11 which compares curves of $C_L/\sqrt{s/c_o}$ plotted against α for the uncambered model, $(C_L - 0.1)/\sqrt{s/c_o}$ plotted against $(\alpha - 5.80^{\circ})$ for the cambered model, and the corresponding Peckham curve[4] for flat plate wings.

3.3 Pitching moment characteristics

Fig.12 shows the pitching-moment coefficient about the mean quarter chord point plotted against lift coefficient for both models. It can be seen that the curve for the uncambered wing is nearly a straight line, but the curve of the cambered wing exhibits a loss of stability near the design point, which is recovered at higher lift coefficients. The position of the aerodynamic centres and centres of pressure are plotted against lift coefficient in Figs.13 and 14 and show variations up to 7% root chord around the design point for cambered wings.

It is suggested that the loss of stability is caused by the movement of the areas of suction associated with the vortices over the cambered form of the wing. At incidences just above the design point, when the vortex patterns are narrow and close to the leading edges, the area of suction near the trailing edge is sidewards and near the apex it is upwards; hence the centre of lift is well forward. At higher incidences the vortices are further inboard and are therefore over the flatter part of the wing; the vector area of the suction is less affected by the camber allowing the centre of lift to return to the normal position.

3.4 Drag characteristics

The drag is plotted against incidence in Fig.15 and shows typical curves, that of the cambered wing being displaced by an angle less than the incidence of the design point. Fig.16 shows the lift-drag ratios plotted against lift coefficient. There is a substantial gain in L/D by the use of camber, L/D maximum increasing from 7.6 to 11.2. This gain is principally due to the shift of the minimum drag point to $\alpha = 4^{\circ}$ (only 2° below the design point) with only a small increase in the minimum drag coefficient. L/D is also improved by the reduction of the 'drag due to lift factor' of the cambered wing, defined as $K = \pi A(C_D - C_{D\ MIN})/(C_L - C_{L_{D\ MIN}})^2$, and plotted against C_L in Fig.17. K is much reduced at low lift coefficients by camber from values approaching 2.0 to less than 1.13, very near to the theoretical minimum of 1.0.

3.5 Lateral characteristics

The sideforces, yawing moments and rolling moments about the quarter chord point of the uncambered and the cambered wing are plotted against angle of sideslip β for various incidences in Figs.18 to 23. These curves are for the most part reasonably linear and the derivatives $dC_\ell/d\beta$, $dC_n/d\beta$ and $dC_Y/d\beta$ were therefore obtained from the slope at $\beta = 0$; they are plotted against C_L in Figs.24, 25 and 26.

3.5.1 Rolling moments

The rolling moment derivative for the cambered wing is less than the uncambered wing at a given C_L. The difference amounts to a 10% reduction at $C_L = 0.5$ and there is a slight kink in the curve of the cambered wing at $C_L = 0.3$. A larger difference might have been expected as the flow patterns differ so much when yawed. However if the derivatives were plotted against incidence instead of C_L the curves would look very different, for at $\alpha = 15^\circ$ the derivative of the cambered wing is 42% less than that for the uncambered wing.

3.5.2 Sideforce

The sideforce derivative of the cambered wing shows more variation with C_L than the uncambered wing, being negative for $C_L < 0.3$ and positive for $C_L > 0.3$. This change of sign is caused by the increasing suction near the windward leading edge as the separation develops with incidence.

3.5.3 Yawing moments

The yawing moment derivatives of both wings are small, the uncambered model giving a result similar to that in Ref.4, but the cambered model has a derivative of opposite sign within the range tested. The curve of the cambered model also shows a kink at $C_L = 0.3$ of a similar nature to that shown by other derivatives.

4 CONCLUSIONS

Surface flow experiments show that the design requirement of completely attached flow at one incidence on the cambered wing, has been realised, and in addition show interesting comparisons with the behaviour of the uncambered wing at yaw. The flow patterns, summarised in Fig.9 in terms of cross-flow, bear superficial resemblances to two-dimensional flow over inverted U - section and flat-plate wings.

The lift curves of the wings are identical in shape but are displaced from each other by the design incidence of 5.8° and design $C_L = 0.1$. This causes a loss of lift of $\Delta C_L = 0.13$ or 27% at $\alpha = 15^\circ$.

There is a loss of stability near the design point of the cambered wing which is recovered at higher incidences and, below the design incidence and

The lateral characteristics of both cambered and uncambered wings are normal for slender wings, the largest lateral derivative being $dC_\ell/d\beta$; $dC_n/d\beta$ and $dC_Y/d\beta$ are small. The rolling-moment derivative of the cambered wing is not much less than the uncambered wing when plotted against C_L but is much less on an incidence basis, the value for the cambered model being 42% less at $\alpha = 15^\circ$.

LIST OF SYMBOLS

A	Aspect ratio
c_o	Root chord
$\bar{\bar{c}}$	Aerodynamic mean chord
b	Overall wing span
q	Kinetic pressure
S	Wing planform area
s	Semi span
α	Angle of incidence
β	Angle of sideslip
C_L	Lift coefficient = Lift/q S
C_D	Drag coefficient = Drag/q S
$C_{D\ MIN}$	Minimum value of the drag coefficient
C_m	Pitching moment coefficient = Moment/q S $\bar{\bar{c}}$
C_n	Yawing moment coefficient = Moment/q S b
C_ℓ	Rolling moment coefficient = Moment/q S b
C_Y	Sideforce coefficient = Sideforce/q S
$dC_\ell/d\beta$, $dC_n/d\beta$, $dC_Y/d\beta$	Lateral derivatives determined as the slope of the coefficient with respect to β, in radians
ν, η_{OT}	Parameters used by Weber[2] to describe the type of camber etc.

LIST OF REFERENCES

No.	Author(s)	Title, etc
1	Peckham, D.H., Atkinson, S.A.	Preliminary results of low speed tunnel tests on a gothic wing of aspect ratio 1.0. A.R.C. C.P.508. April, 1957.
2	Weber, J.	Design of warped slender wings with the attachment line along the leading edge. A.R.C. 20,051. September, 1957.
3	Maskell, E.C.	Flow separation in three dimensions. Published in Proc. Roy. Soc. A.R.C. 18,063. November, 1955.
4	Peckham, D.H.	Low-speed wind-tunnel tests on a series of uncambered slender pointed wings with sharp edges. A.R.C. R. & M. 3186. December, 1958.
5	Maskell, E.C., Weber, J.	On the aerodynamic design of slender wings. A.R.C. 20,610. August, 1956.

TABLE 1

Geometry of models

Span	$b = 2s$	3.0 ft
Root chord	c_o	6.0 ft
Aerodynamic mean chord	$\bar{\bar{c}}$	4.5 ft
Wing area	S	12.0 sq ft
Aspect ratio	A	0.75
Position of $\bar{\bar{c}}/4$ pt. from apex		2.63 ft = 44% c_o
Thickness: chord ratio	t/c_o	$8\frac{1}{4}\%$
Max thickness at		40% c_o from apex
Root chord thickness form[5]		Bi-convex
Cross-section[5]	Uncambered model	Diamond
	Cambered model	Diamond thickness form on a cambered base line
Camber[1,5]	Design $C_L = 0.1$ using Weber's method[2]	$\nu = 2\ \eta_{OT} = 0.8$

W.T.2078.C.P.576.K3 - Printed in England

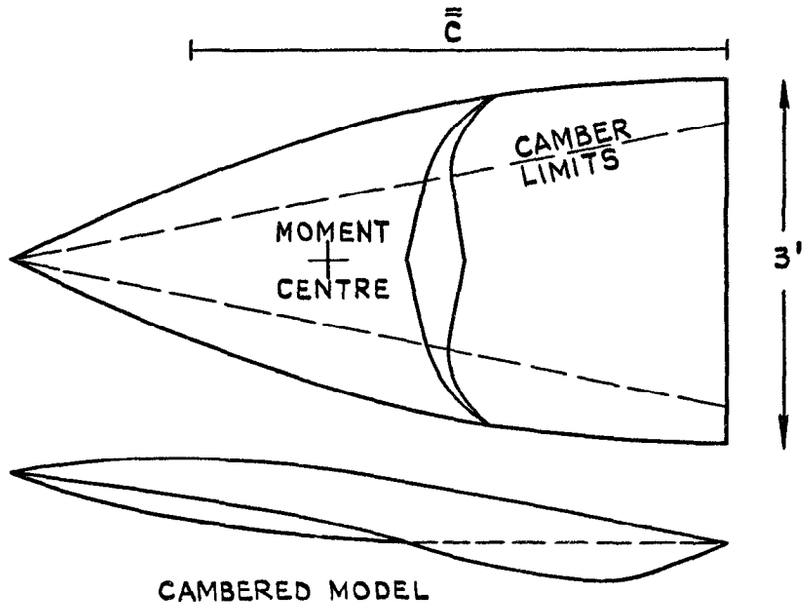

CAMBERED MODEL

6'

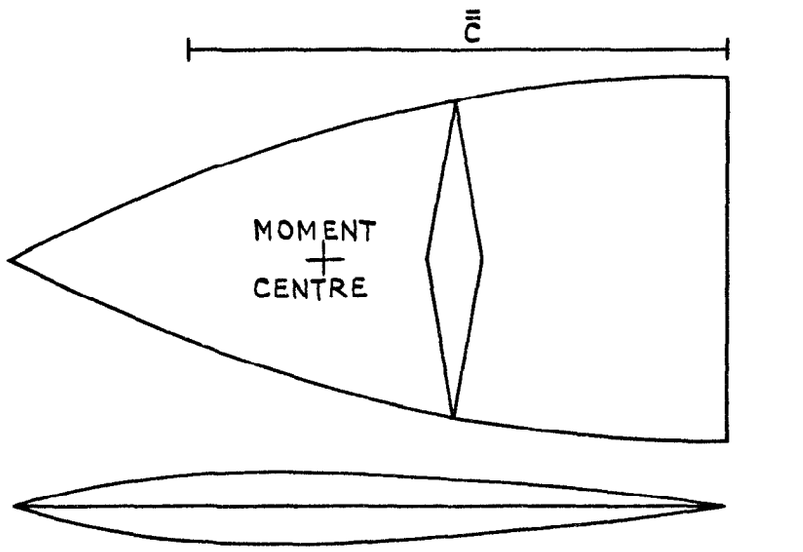

UNCAMBERED MODEL

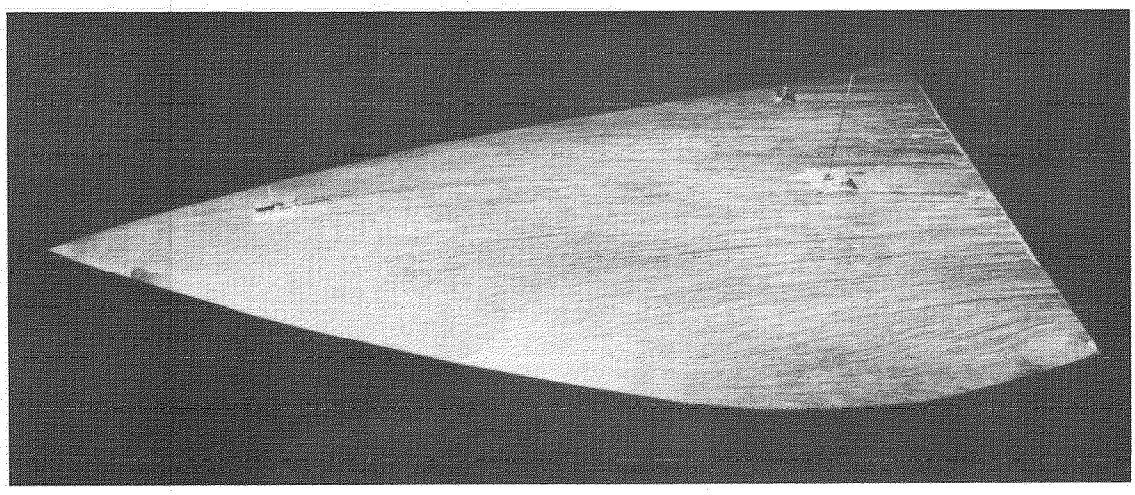

$\alpha = 0^{\circ}$ $\beta = 0^{\circ}$

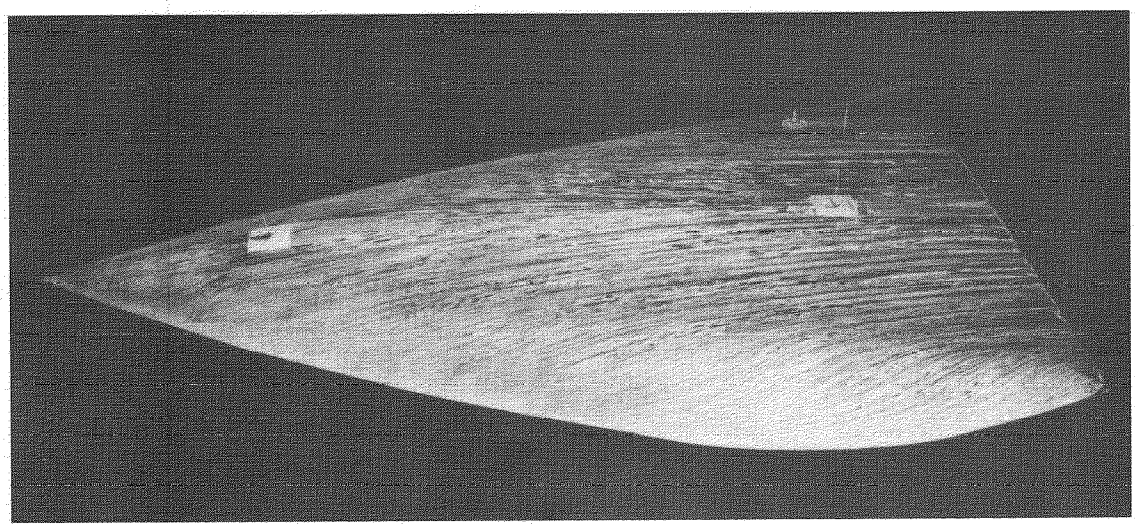

$\alpha = 2^{\circ}$ $\beta = 0^{\circ}$

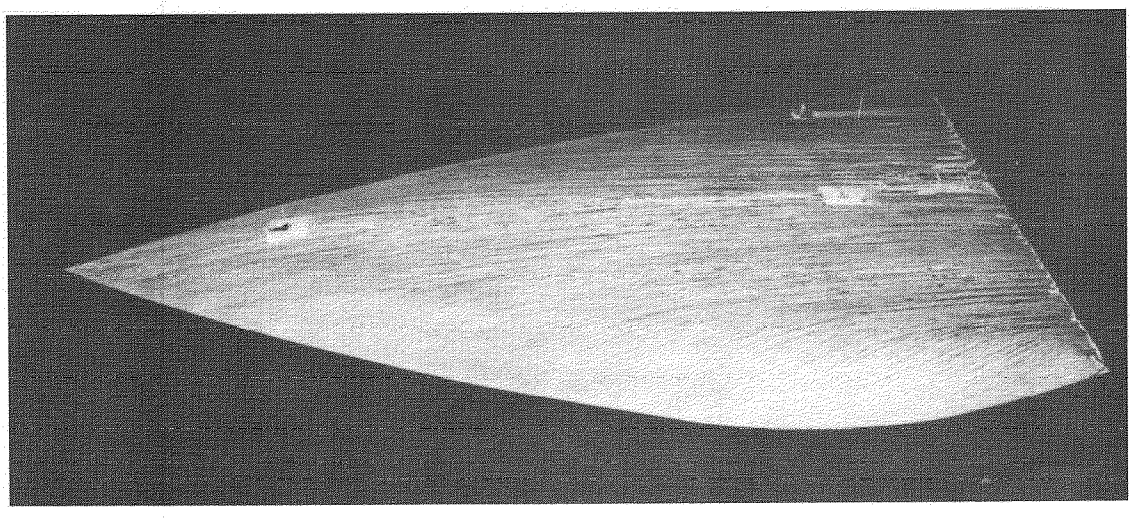

$\alpha = 4^{\circ}$ $\beta = 0^{\circ}$

FIG 2 UPPER SURFACE FLOW PATTERNS ON CAMBERED GOTHIC WING

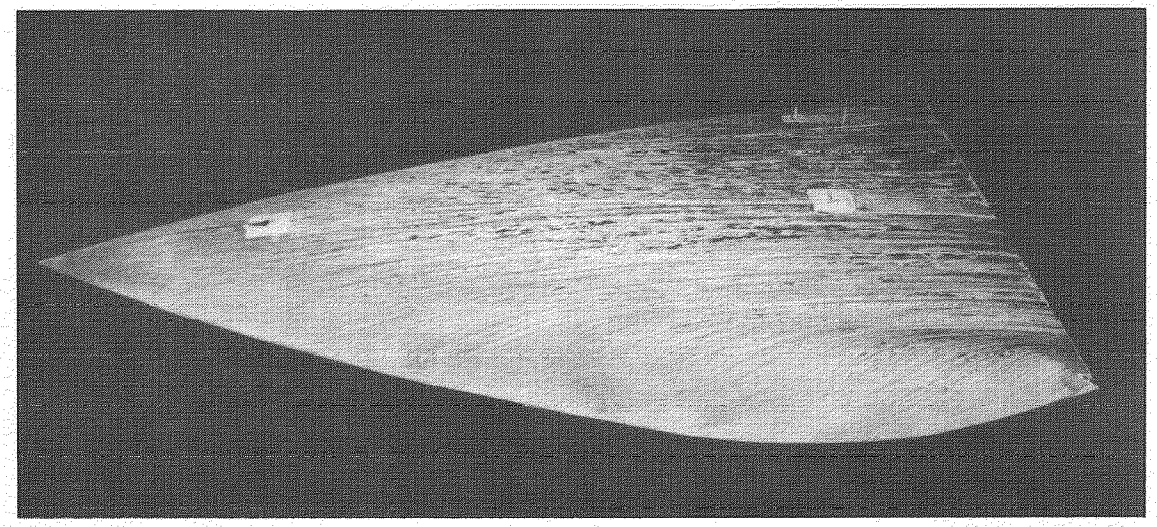

$\alpha = 6^{\circ}$ $\beta = 0^{\circ}$

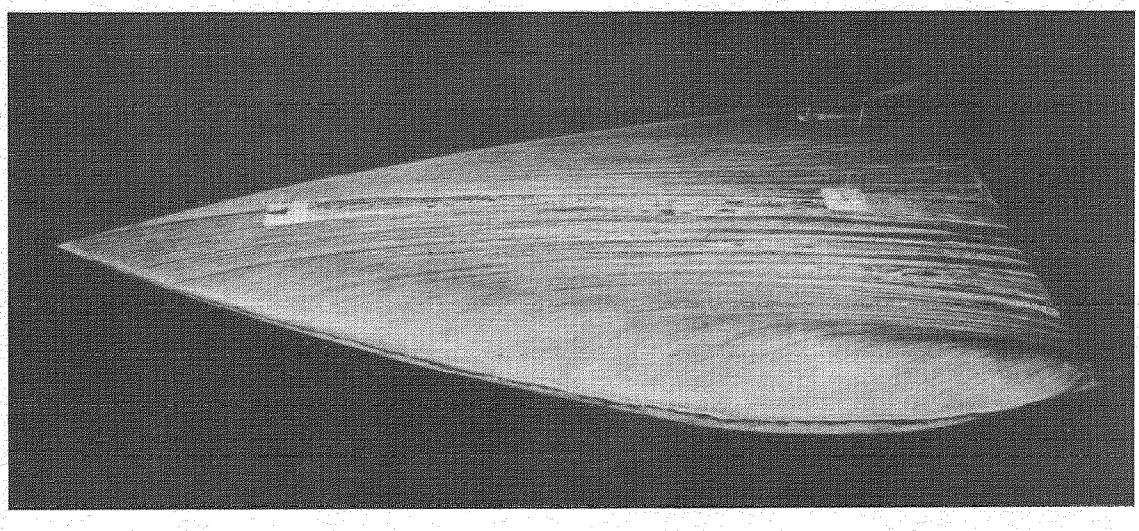

$\alpha = 8^{\circ}$ $\beta = 0^{\circ}$

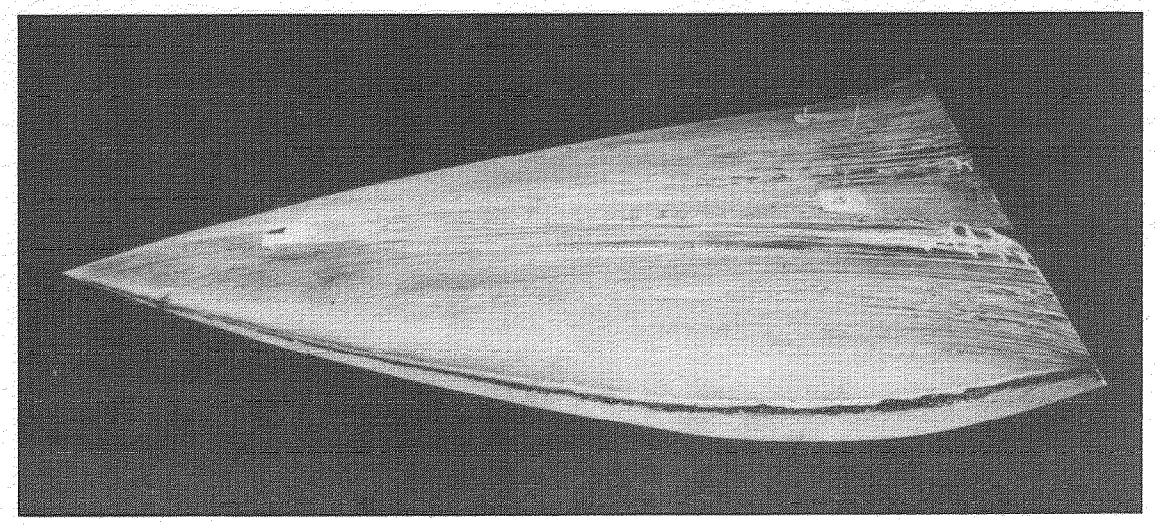

$\alpha = 12^{\circ}$ $\beta = 0^{\circ}$

FIG.3. UPPER SURFACE FLOW PATTERNS ON CAMBERED GOTHIC WING

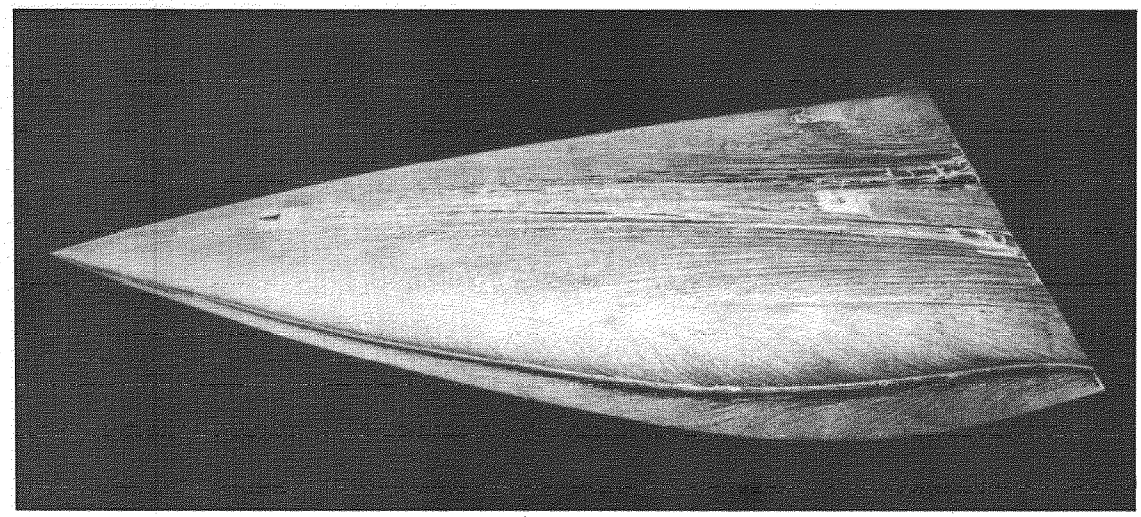

$\alpha = 15^{\circ}$ $\beta = 0^{\circ}$

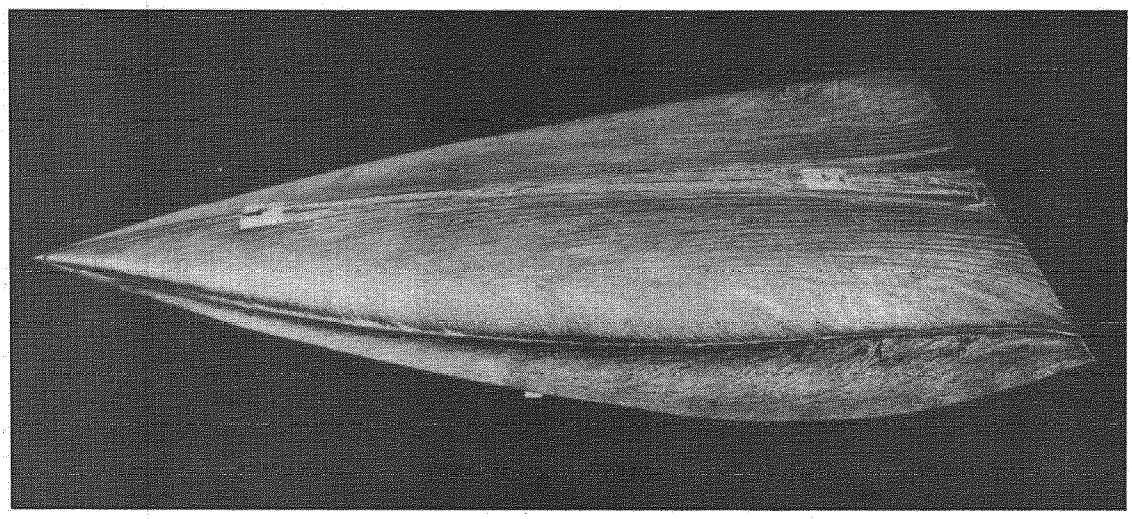

$\alpha = 20^{\circ}$ $\beta = 0^{\circ}$

FIG.4. UPPER SURFACE FLOW PATTERNS ON CAMBERED GOTHIC WING

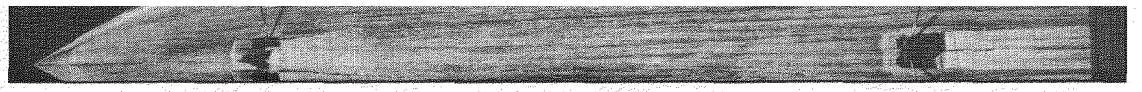

$\alpha = 2^{\circ}$ $\beta = 0^{\circ}$ LOWER SURFACE

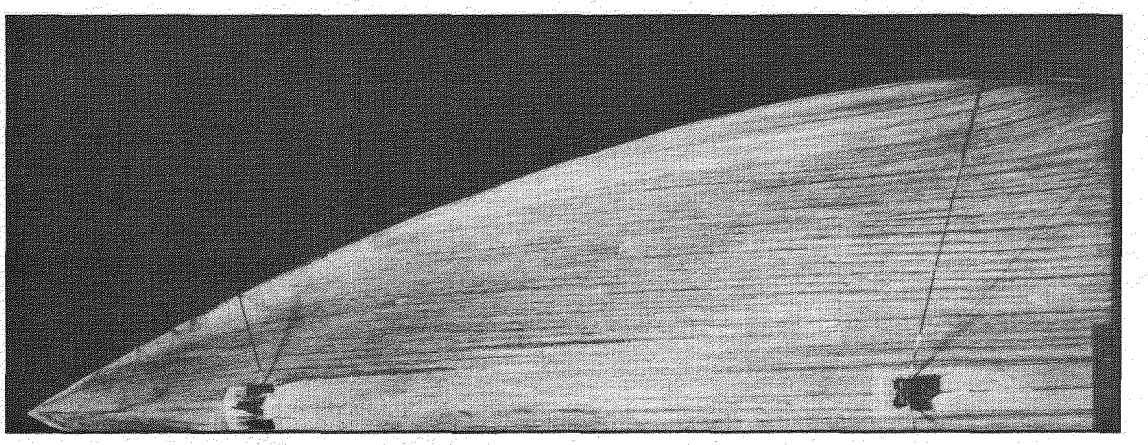

$\alpha = 4^{\circ}$ $\beta = 0^{\circ}$ LOWER SURFACE

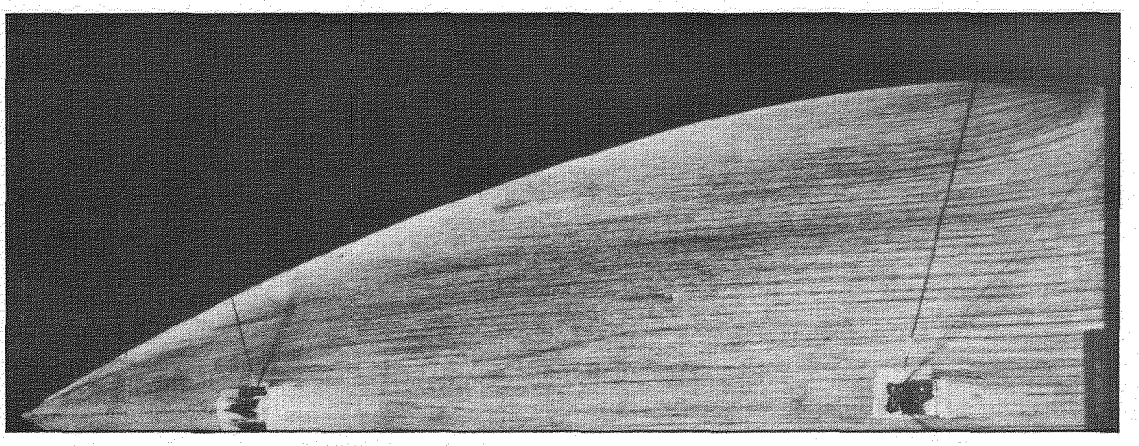

$\alpha = 8^{\circ}$ $\beta = 0^{\circ}$ LOWER SURFACE

FIG.5. LOWER SURFACE FLOW PATTERNS ON CAMBERED GOTHIC WING

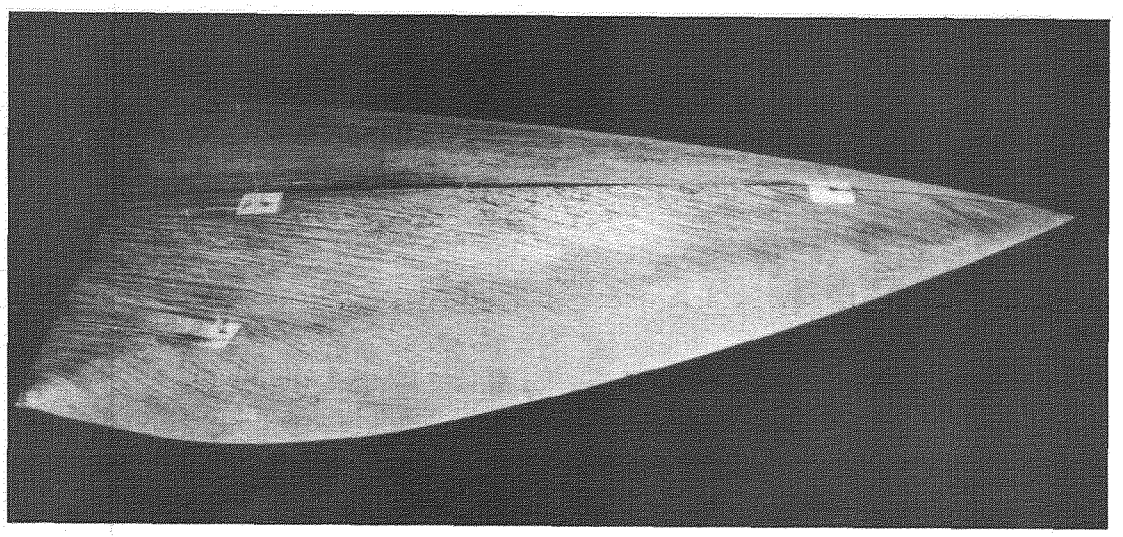

$\alpha = 0^{\circ}$ $\beta = 10^{\circ}$ VIEW FROM STARB'D SIDE

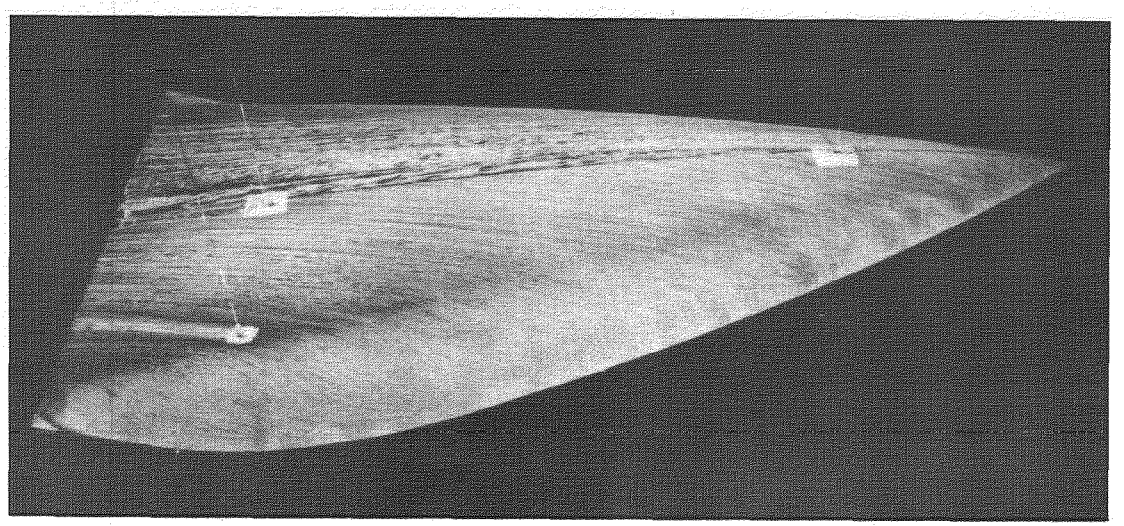

$\alpha = 4^{\circ}$ $\beta = 10^{\circ}$ VIEW FROM STARB'D SIDE

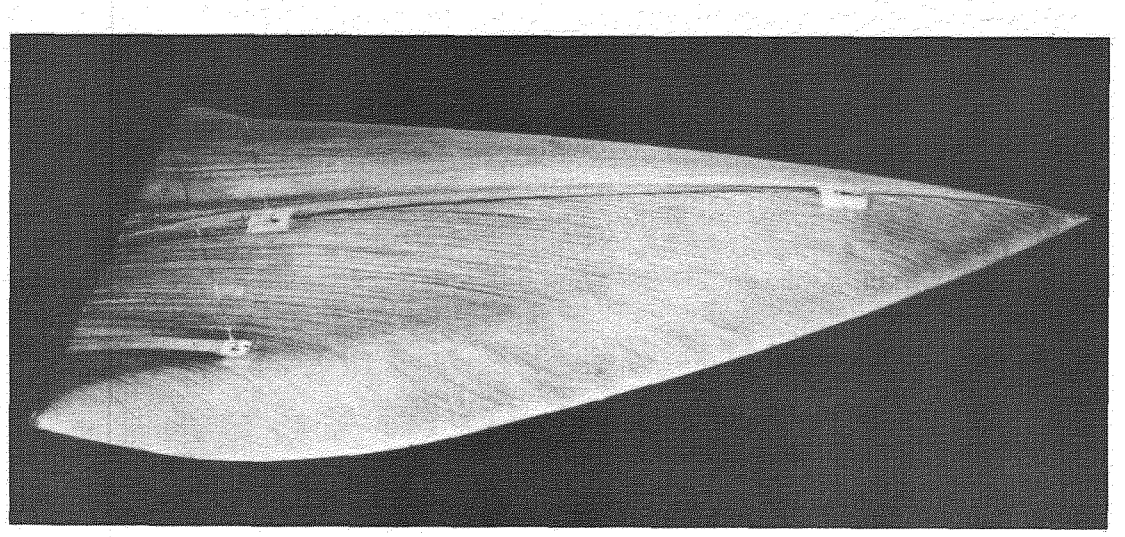

$\alpha = 8^{\circ}$ $\beta = 10^{\circ}$ VIEW FROM STARB'D SIDE

FIG.6. UPPER SURFACE FLOW PATTERNS ON CAMBERED GOTHIC WING AT YAW

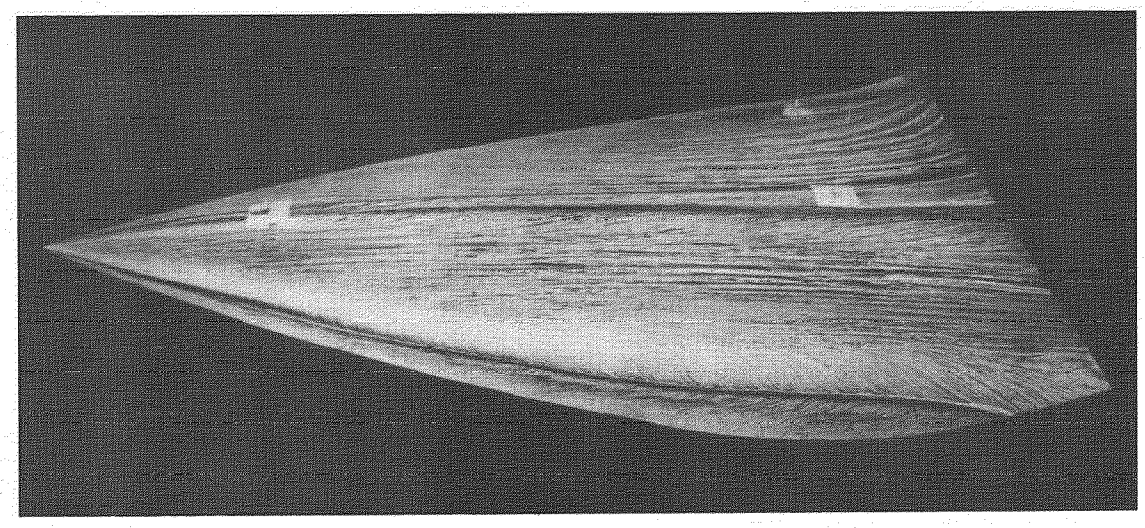

$\alpha = 12^{\circ}$ $\beta = 10^{\circ}$ VIEW FROM PORT SIDE

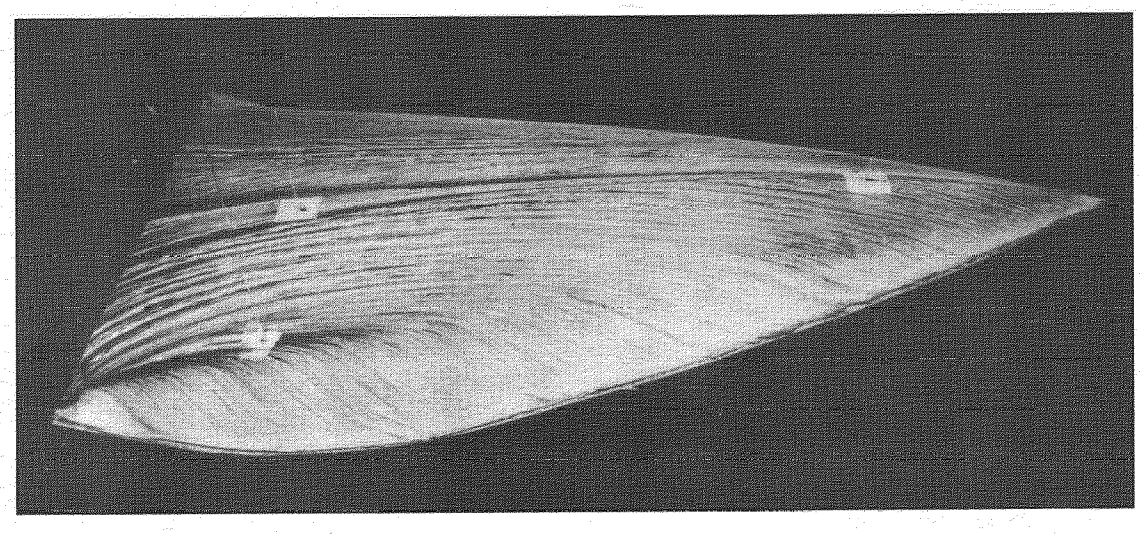

$\alpha = 12^{\circ}$ $\beta = 10^{\circ}$ VIEW FROM STARB'D SIDE

FIG.8. UPPER SURFACE FLOW PATTERNS ON CAMBERED GOTHIC WING AT YAW

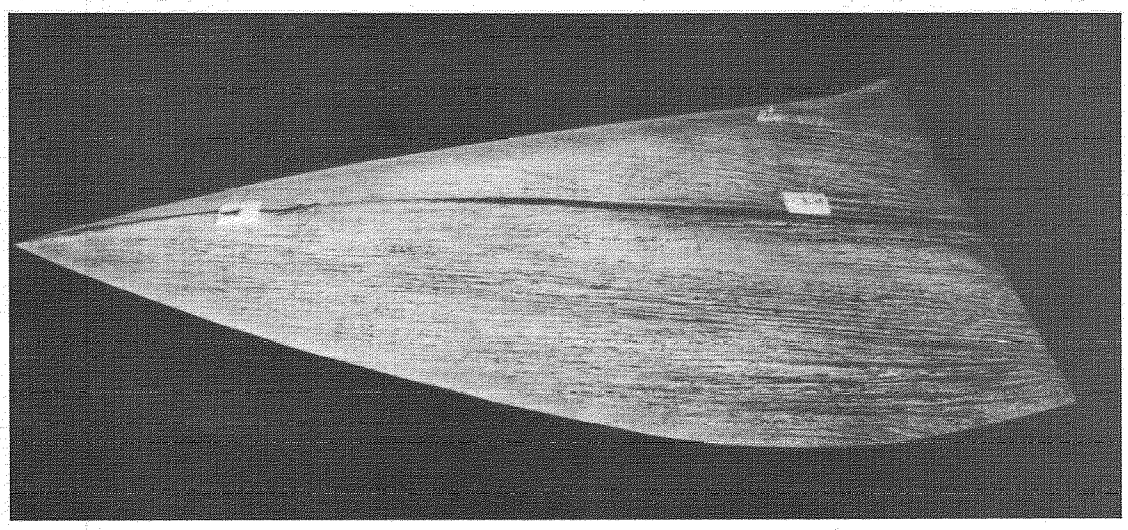

$\alpha = 0^{\circ}$ $\beta = 10^{\circ}$ VIEW FROM PORT SIDE

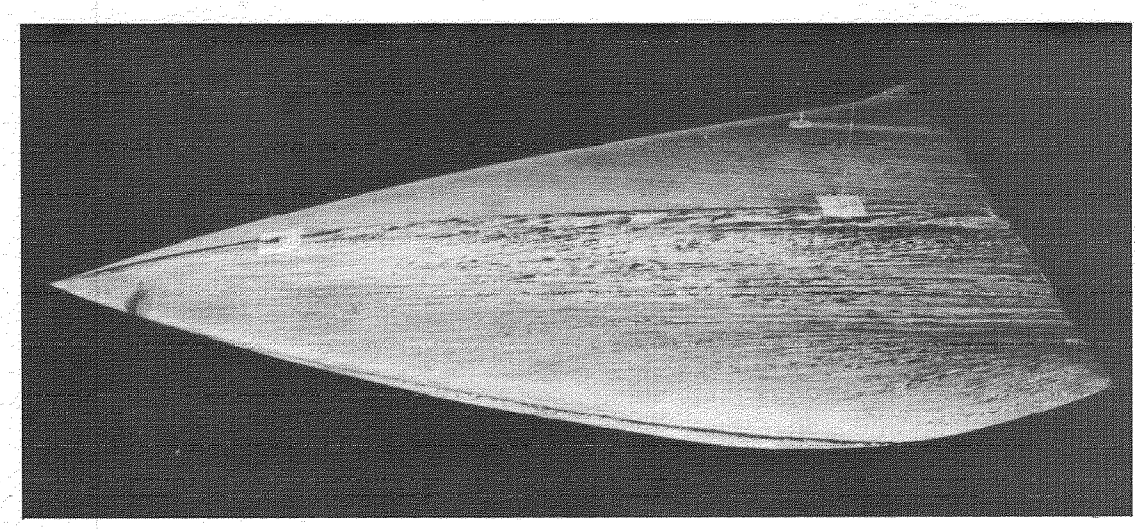

$\alpha = 4^{\circ}$ $\beta = 10^{\circ}$ VIEW FROM PORT SIDE

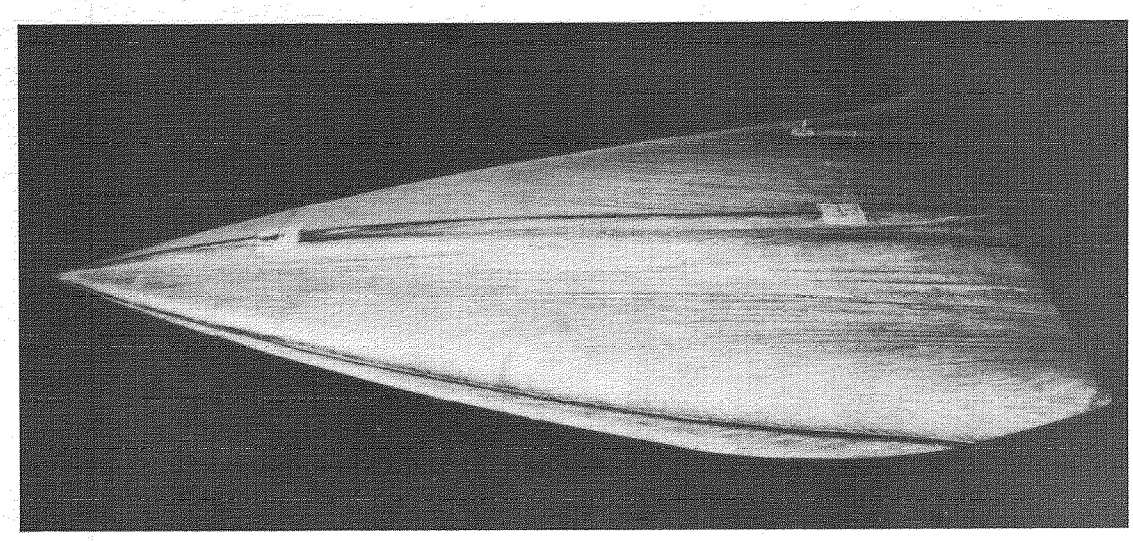

$\alpha = 8^{\circ}$ $\beta = 10^{\circ}$ VIEW FROM PORT SIDE

FIG.7. UPPER SURFACE FLOW PATTERNS ON AN A = 3/4 CAMBERED GOTHIC WING AT YAW

	UNCAMBERED ZERO YAW	CAMBERED ZERO YAW	UNCAMBERED YAWED	CAMBERED YAWED
MUCH ABOVE DESIGN INCIDENCE	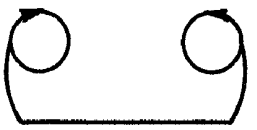	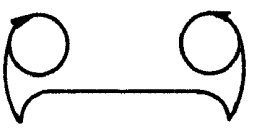	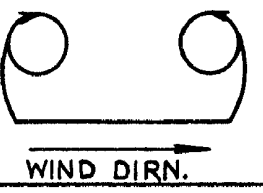	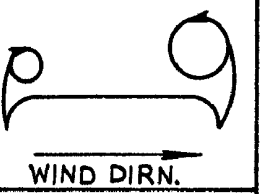
ABOVE DESIGN INCIDENCE		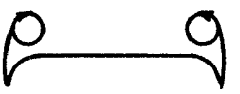		
DESIGN INCIDENCE				
BELOW DESIGN INCIDENCE	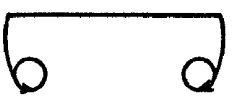		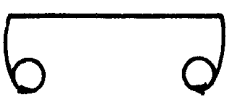	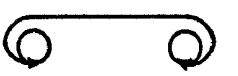

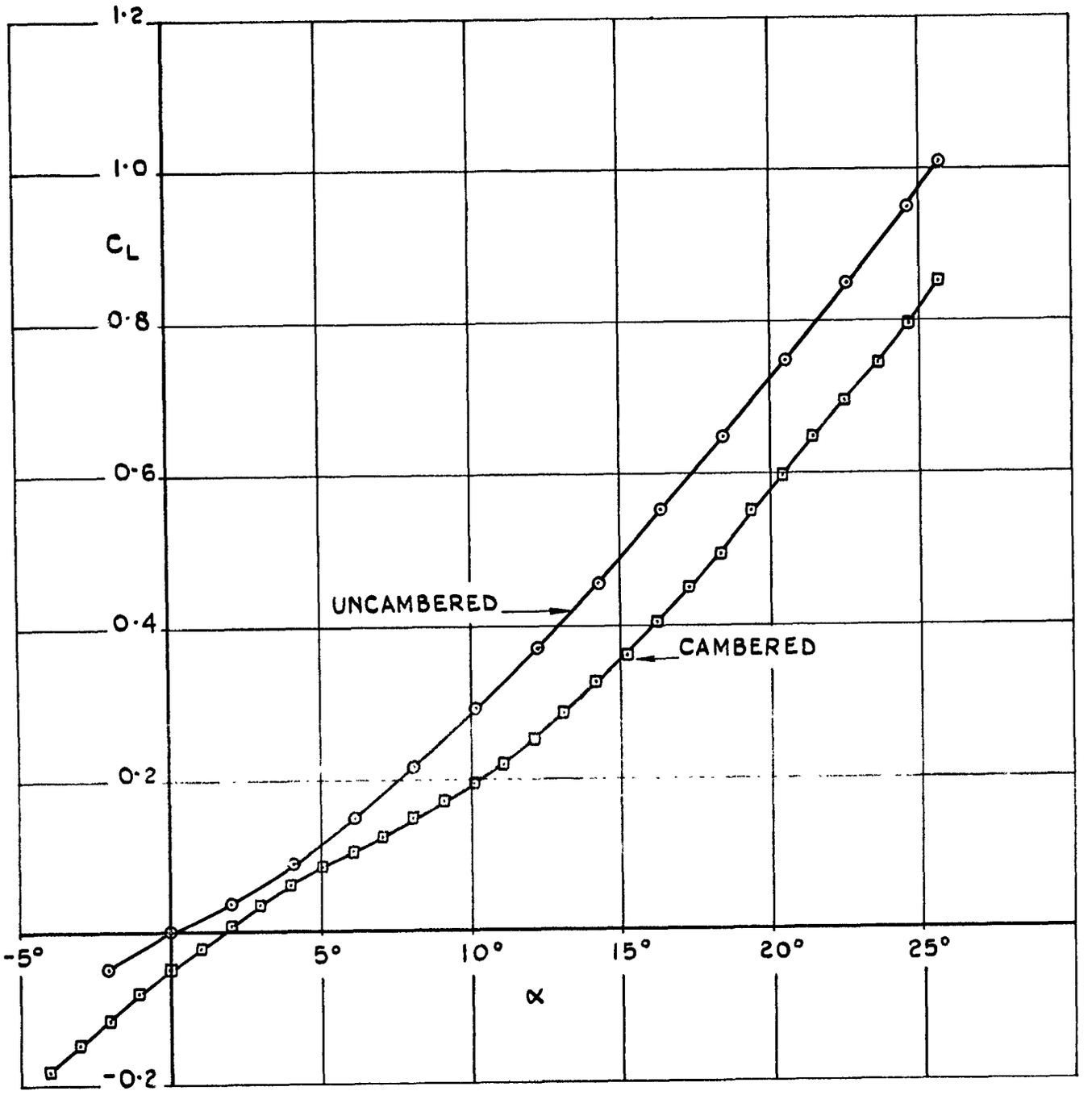

FIG.10. LIFT OF GOTHIC WINGS.

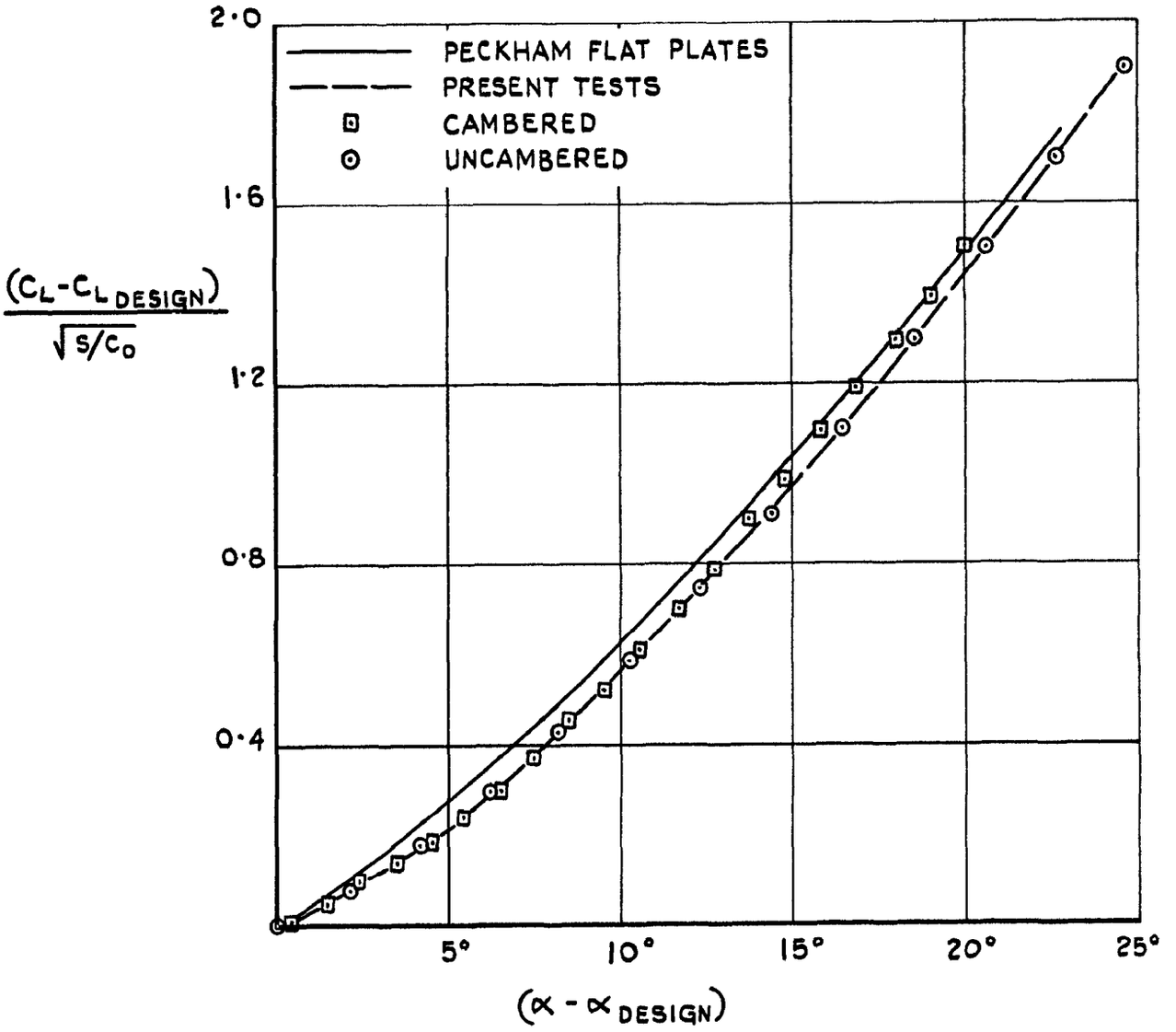

FIG.11. COLLAPSE OF LIFT DATA OF GOTHIC WINGS.

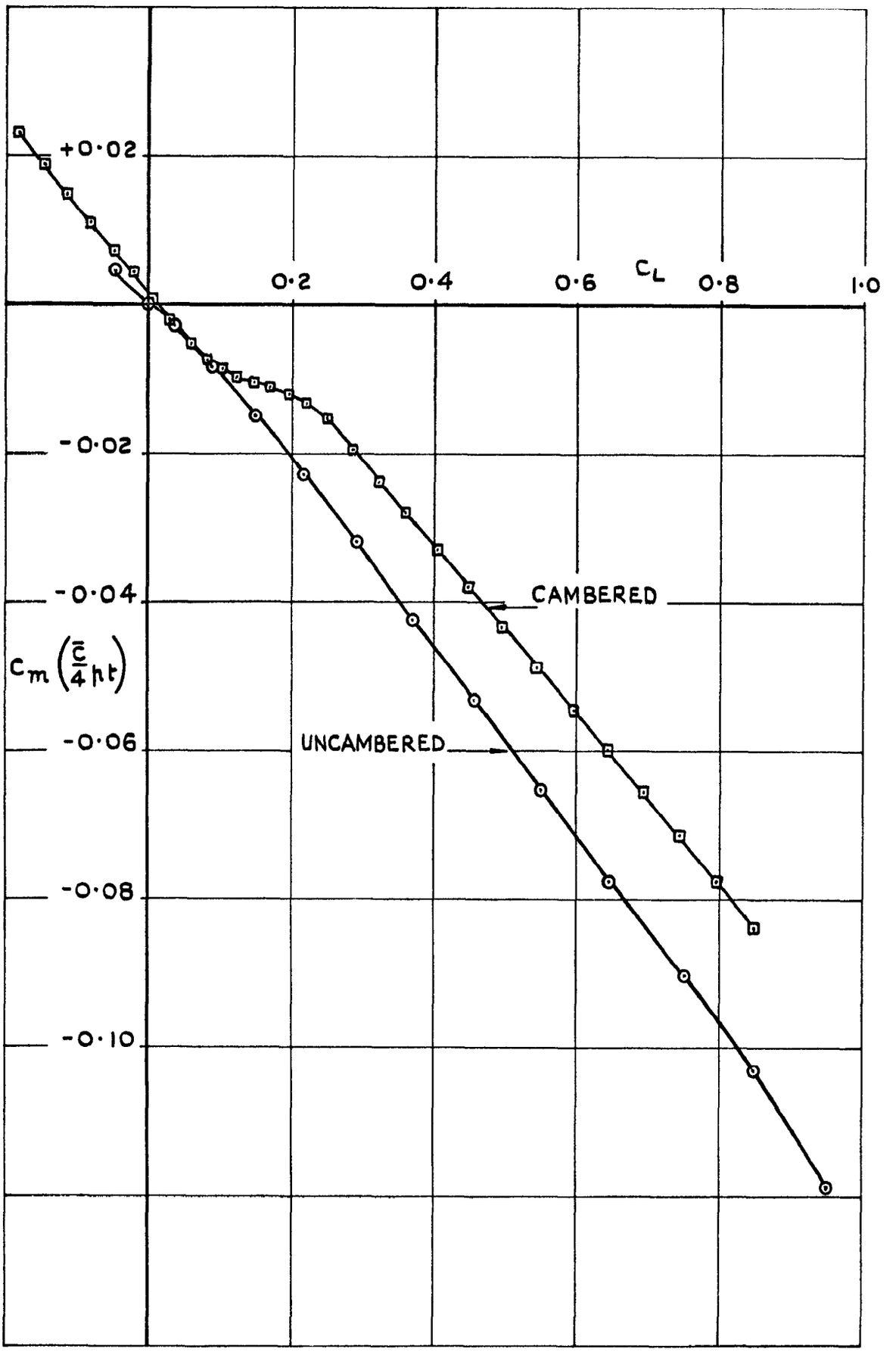

FIG.12. PITCHING MOMENTS OF GOTHIC WINGS.

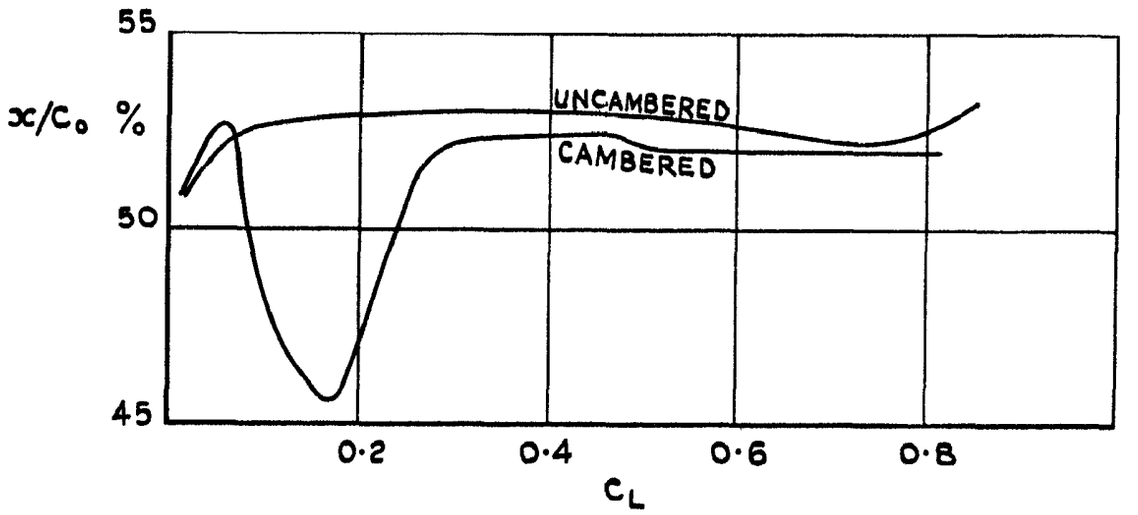

FIG.13. POSITION OF AERODYNAMIC CENTRES FROM THE APEX.

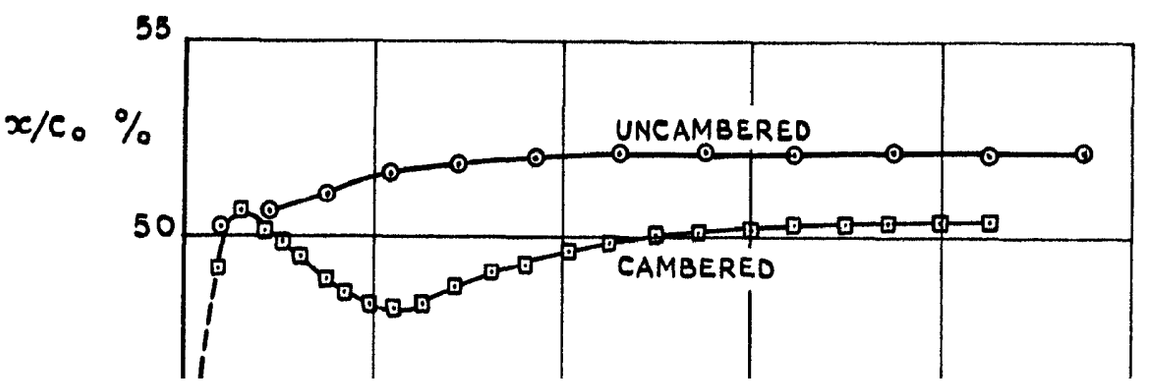

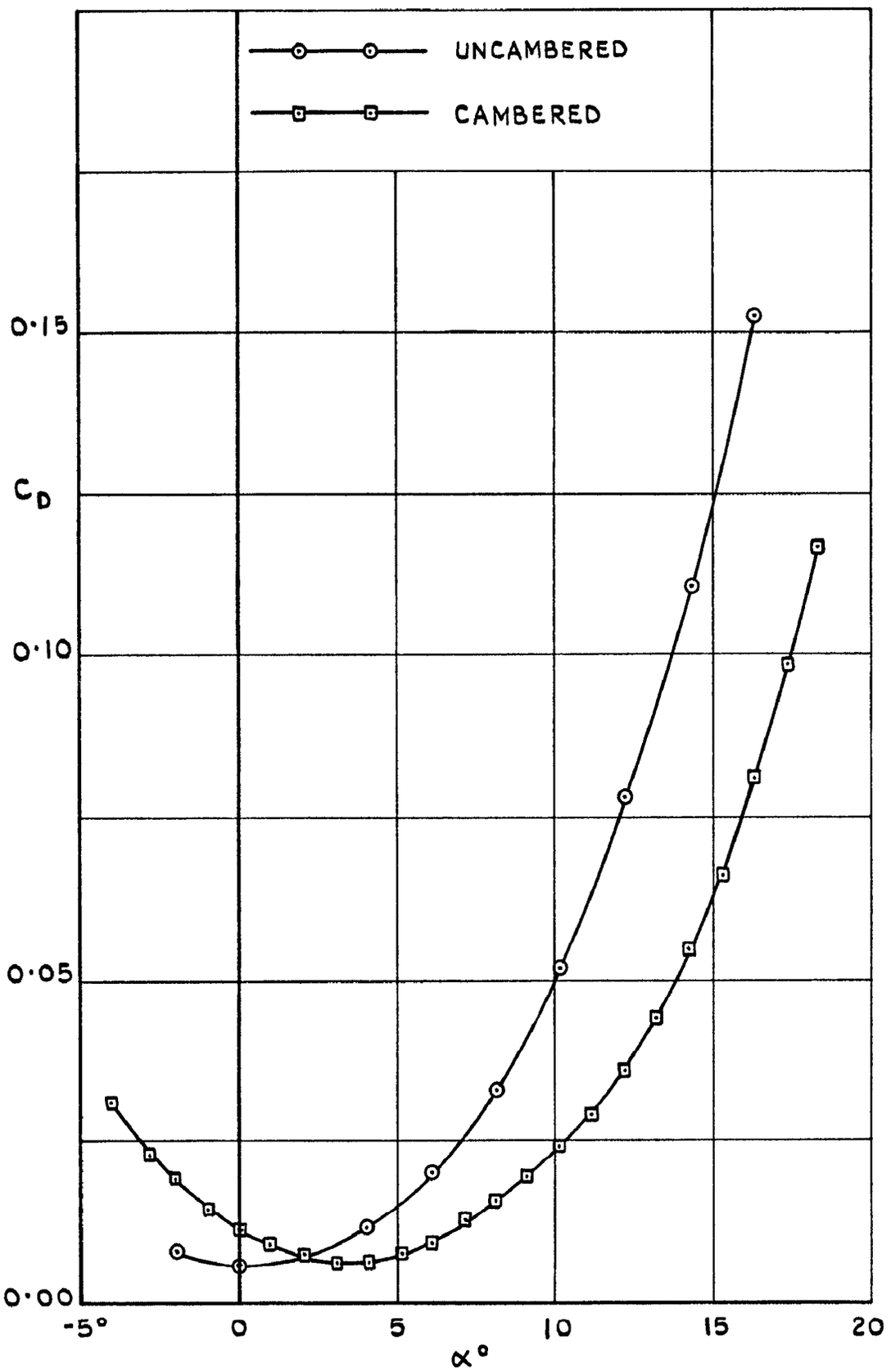

FIG.15. DRAG COEFFICIENTS OF CAMBERED AND UNCAMBERED A = 3/4 GOTHIC WINGS.

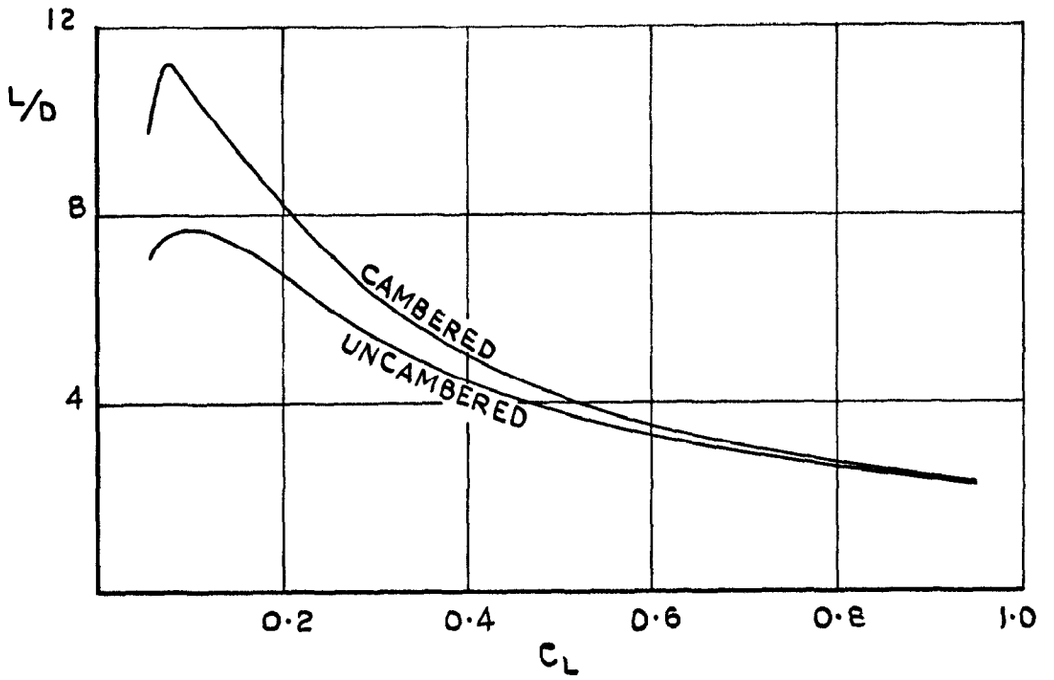

FIG.16. LIFT/DRAG RATIOS OF GOTHIC WINGS.

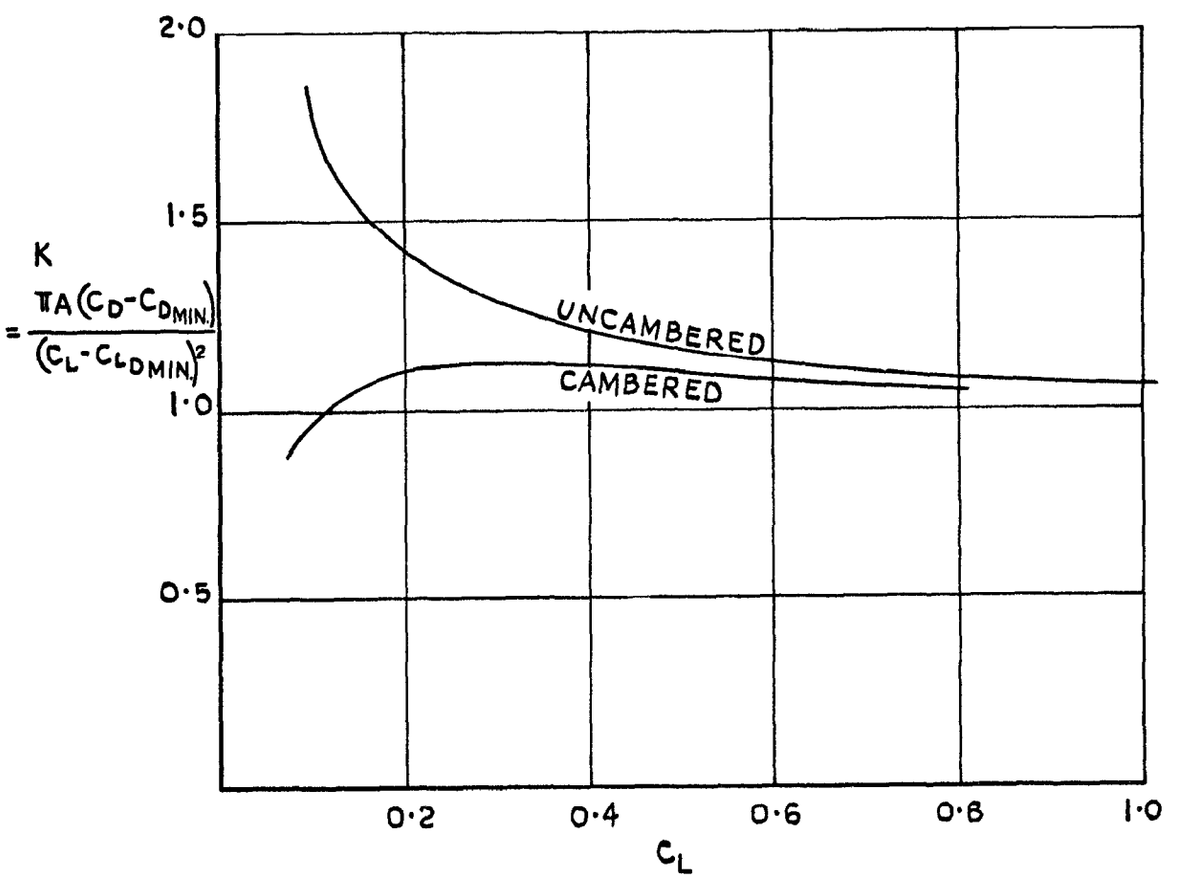

FIG.17. INDUCED DRAG FACTOR OF GOTHIC WINGS.

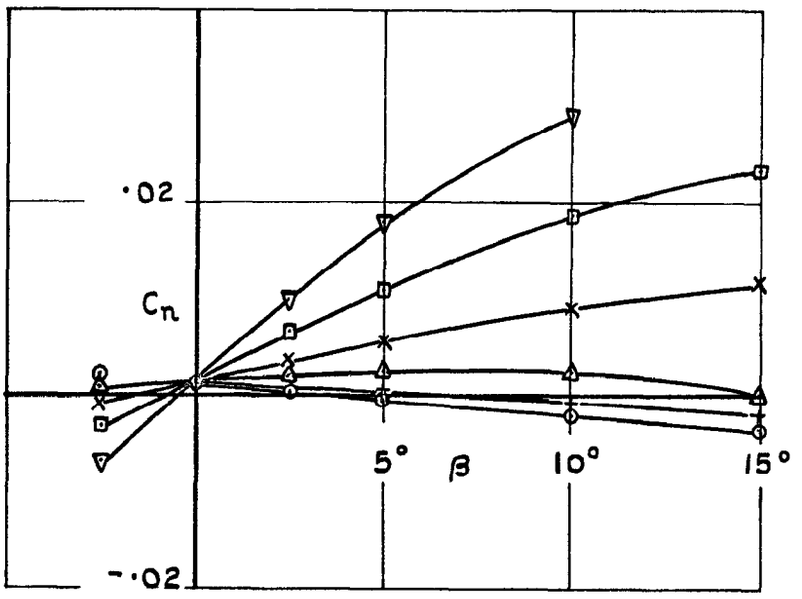

FIG.18. VARIATION OF YAWING MOMENT WITH SIDESLIP FOR THE UNCAMBERED MODEL.

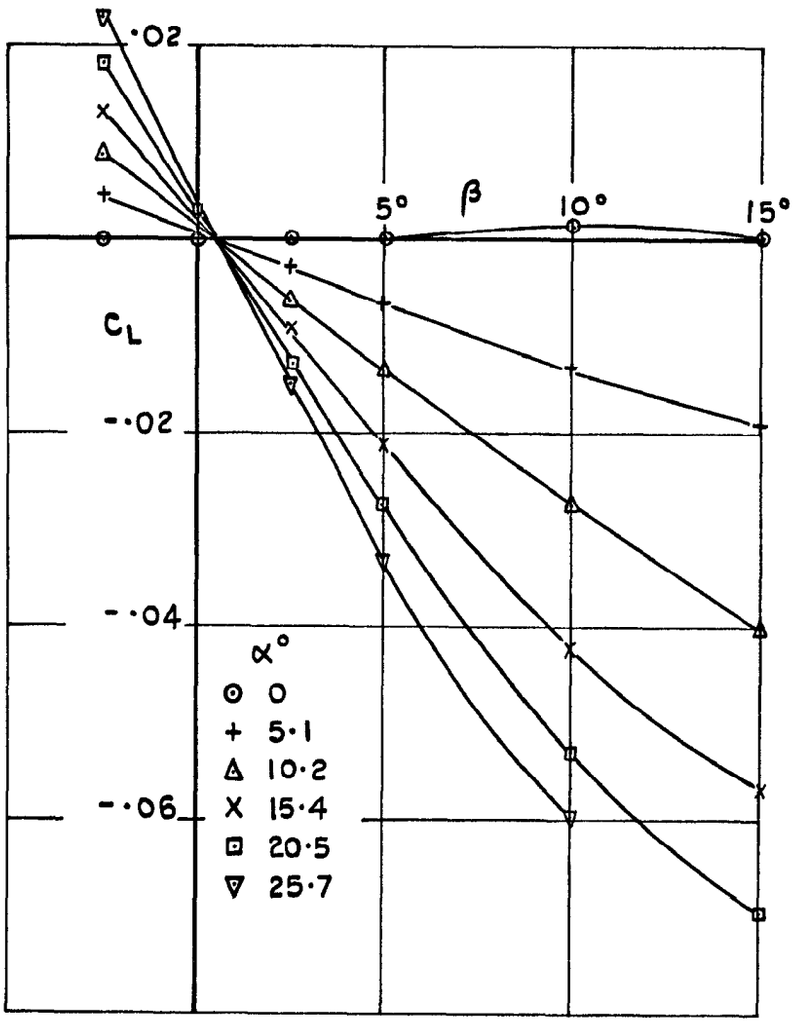

FIG.19. VARIATION OF ROLLING MOMENT WITH SIDESLIP FOR THE UNCAMBERED MODEL.

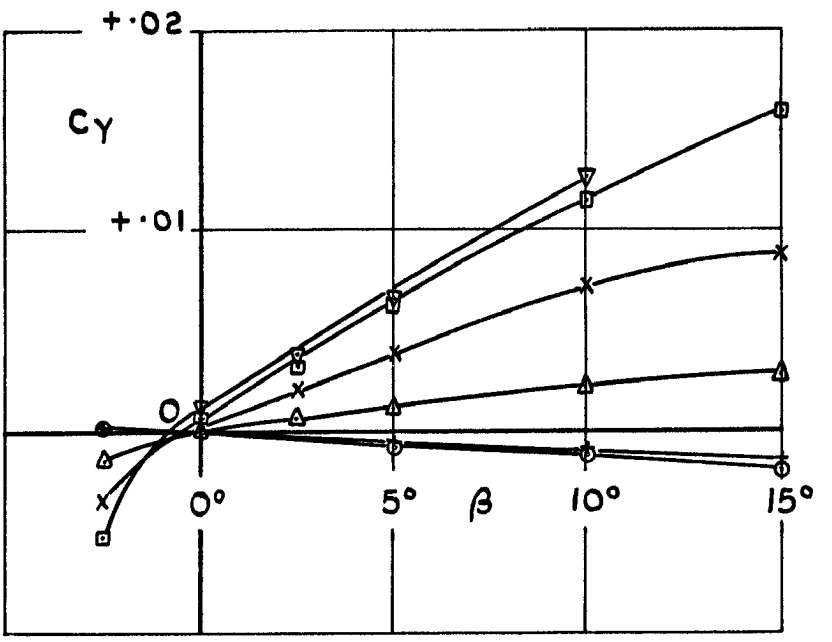

FIG.20. VARIATION OF SIDEFORCE COEFFICIENT WITH SIDE-SLIP FOR THE UNCAMBERED MODEL.

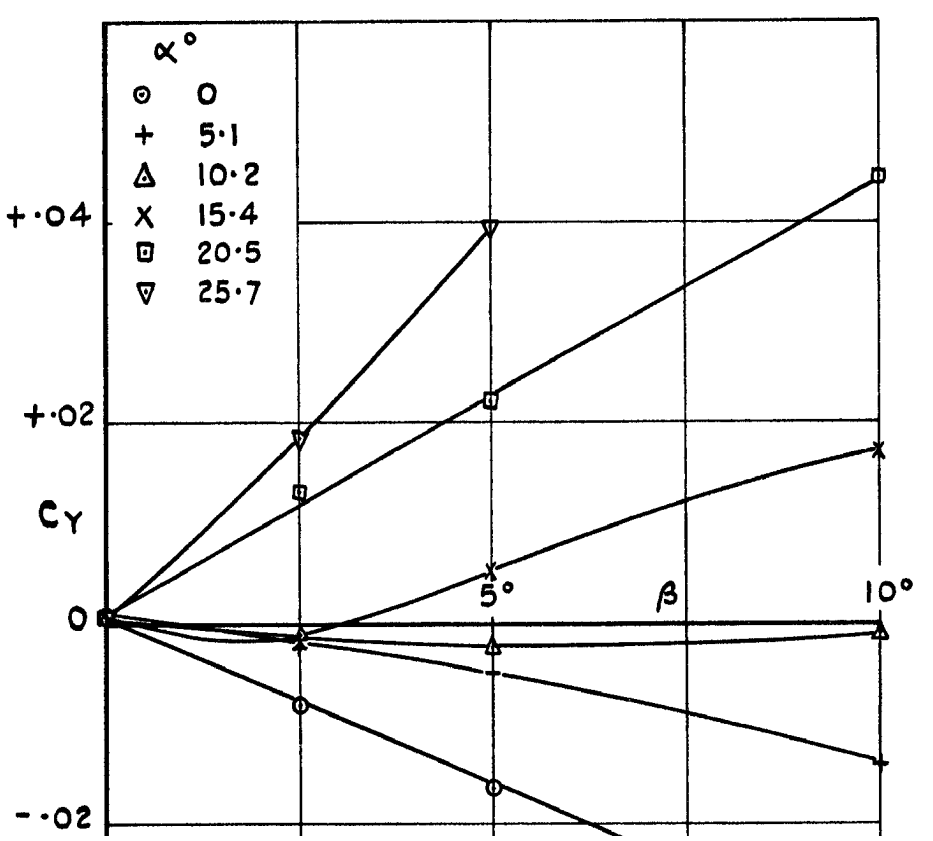

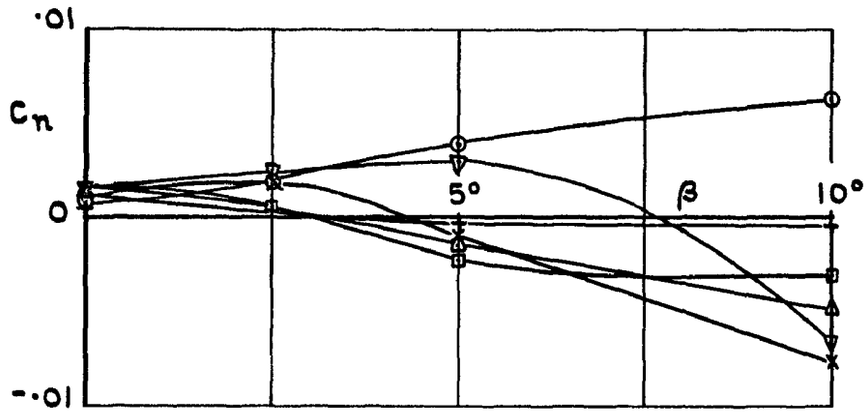

FIG. 22. VARIATION OF YAWING MOMENT COEFFICIENT WITH SIDESLIP FOR THE CAMBERED MODEL.

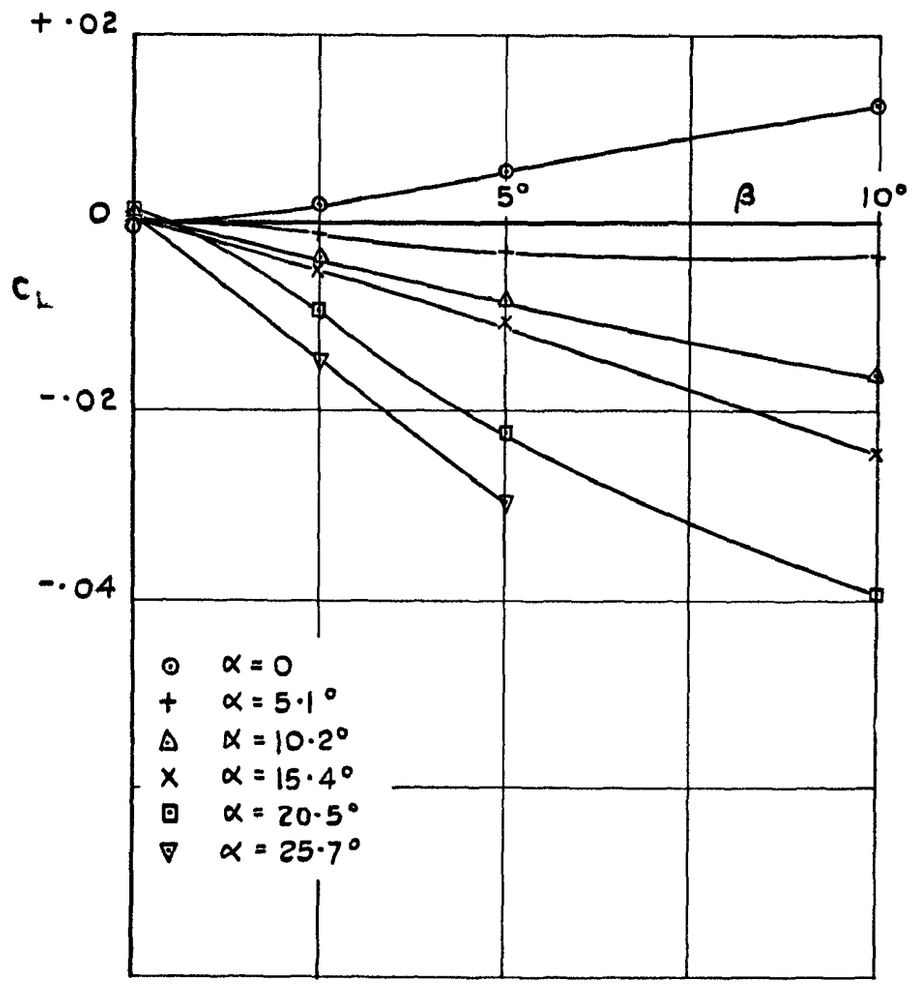

FIG. 23. VARIATION OF ROLLING MOMENT COEFFICIENT WITH SIDESLIP FOR THE CAMBERED MODEL.

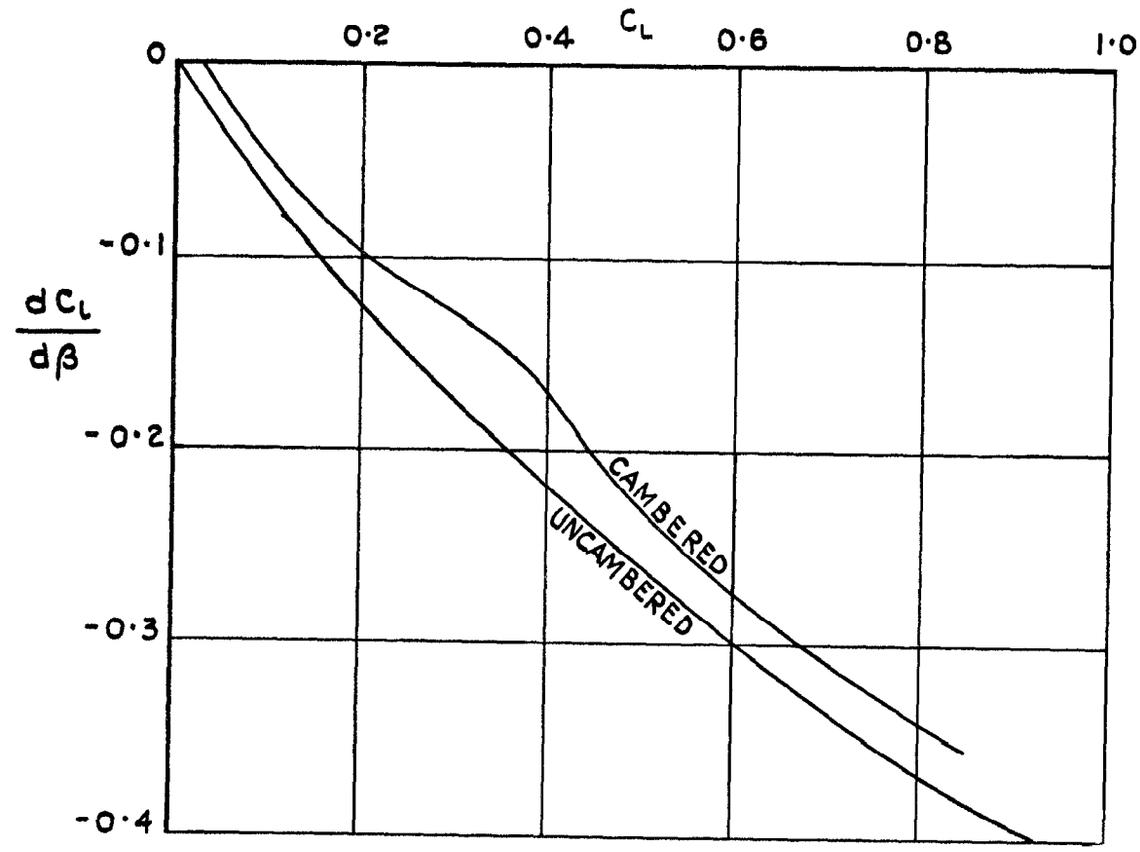

FIG. 24. ROLLING MOMENT DERIVATIVES.

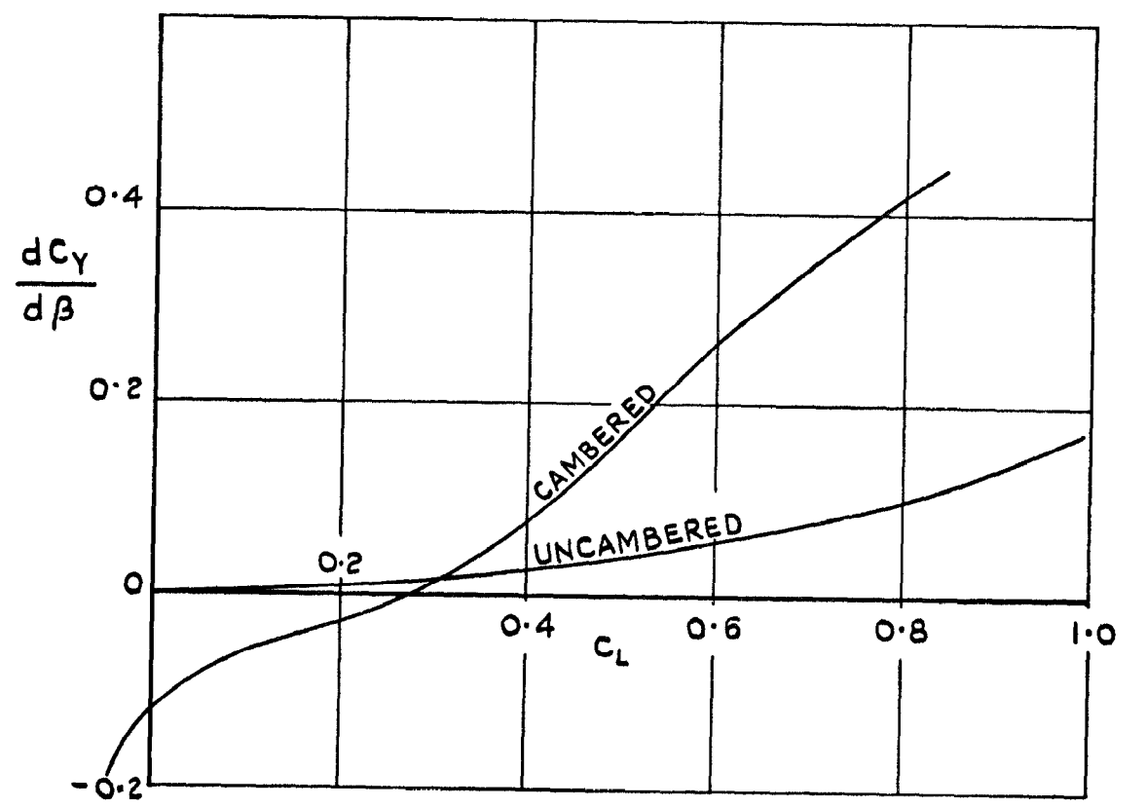

FIG. 25. SIDEFORCE DERIVATIVES.

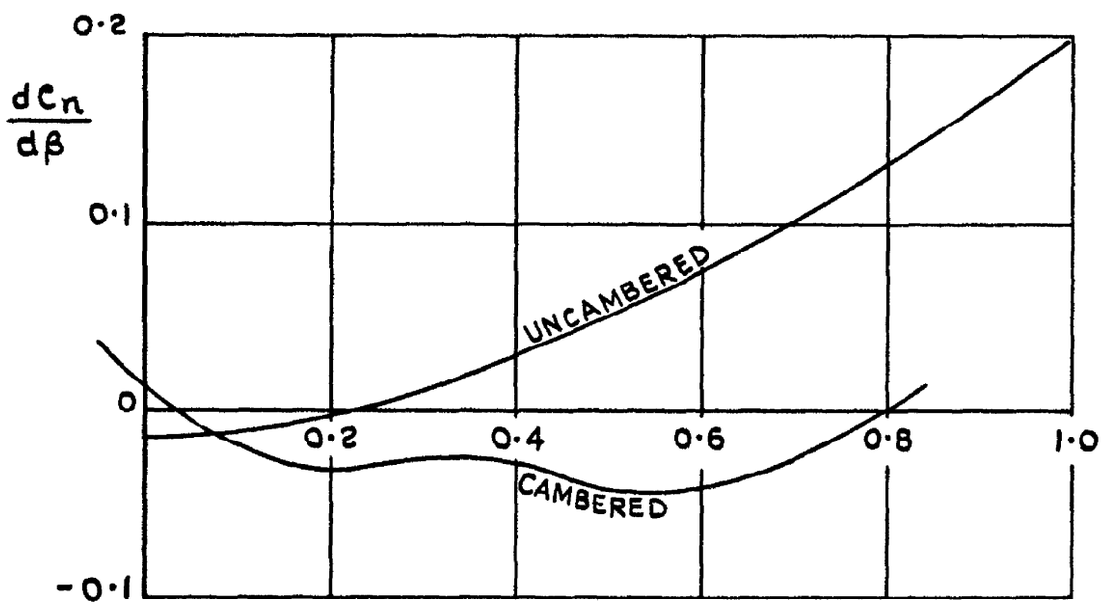

FIG.26. YAWING MOMENT DERIVATIVES.

A.R.C. C.P. No.576

533.693.3 :
533.6.013.413

LOW-SPEED WIND-TUNNEL TESTS ON SHARP-EDGED GOTHIC WING OF ASPECT-RATIO 3/4. Keating, R.F.A. May, 1960.

The results of wind-tunnel tests on a cambered and an uncambered gothic wing are presented. Longitudinal and lateral force measurements were made on both wings, together with oil flow visualisation studies on the cambered wing.

The flow patterns showed that the design requirement of fully attached flow at a small range of incidence of the cambered wing was realised. However, the cambered wing gave less lift than the uncambered version at any prescribed incidence; this loss amounted to $\Delta C_L = -0.13$ at $\alpha = 15^0$ i.e. a loss of 27%. A reduction of stability occurs near the design point which is recovered at higher incidences, otherwise the location of the aerodynamic centres of both wings are the same, namely 0.52 c_0 from the

P.T.O.

A.R.C. C.P. No.576

LOW-SPEED WIND-TUNNEL TESTS ON SHARP
ASPECT-RATIO 3/4. Keating, R.F.A.

The results of wind-tunnel tes
gothic wing are presented. Longitud
were made on both wings, together wi
the cambered wing.

The flow patterns showed that
flow at a small range of incidence o
However, the cambered wing gave less
any prescribed incidence; this loss
i.e. a loss of 27%. A reduction of
which is recovered at higher inciden
aerodynamic centres of both wings ar

A.R.C. C.P. No.576

LOW-SPEED WIND-TUNNEL TESTS ON SHARP
ASPECT-RATIO 3/4. Keating, R.F.A.

The results of wind-tunnel tes
gothic wing are presented. Longitud
were made on both wings, together wi
the cambered wing.

The flow patterns showed that
flow at a small range of incidence o
However, the cambered wing gave less
any prescribed incidence; this loss
i.e. a loss of 27%. A reduction of
which is recovered at higher inciden
aerodynamic centres of both wings ar

apex. The higher L/D obtained with the cambered model is associated with the displacement of the incidence for minimum drag towards the design incidence, without much increase in the value of the minimum drag, together with a reduction in lift-dependent drag.

There is only a small difference in the rolling moment derivative between the cambered and the uncambered model when plotted against C_L. However, at the same incidence, the difference is large, $-dC_\ell/d\beta$ being 42% smaller for the cambered wing at 15° incidence.

apex. The higher L/D obtained with the cambered model is associated with the displacement of the incidence for minimum drag towards the design incidence, without much increase in the value of the minimum drag, together with a reduction in lift-dependent drag.

There is only a small difference in the rolling moment derivative between the cambered and the uncambered model when plotted against C_L. However, at the same incidence, the difference is large, $-dC_\ell/d\beta$ being 42% smaller for the cambered wing at 15° incidence.

Published by
HER MAJESTY'S STATIONERY OFFICE

To be purchased from
York House, Kingsway, London w.c.2
423 Oxford Street, London w.1
13A Castle Street, Edinburgh 2
109 St. Mary Street, Cardiff
39 King Street, Manchester 2
50 Fairfax Street, Bristol 1
2 Edmund Street, Birmingham 3
80 Chichester Street, Belfast 1
or through any bookseller

Printed in England

S.O. CODE No.23-9012-76